 MCB, vol.4, no.2, pp.105-118, 2007

# Geometric Confinement Influences Cellular Mechanical Properties II – Intracellular Variances in Polarized Cells

**Judith Su*, Ricardo R. Brau†, Xingyu Jiang‡, George M. Whitesides§, Matthew J. Lang¶, Peter T. C. So‖**

**Abstract:** During migration, asymmetrically polarized cells achieve motion by coordinating the protrusion and retraction of their leading and trailing edges, respectively. Although it is well known that local changes in the dynamics of actin cytoskeleton remodeling drive these processes, neither the cytoskeletal rheological properties of these migrating cells are well quantified nor is it understand how these rheological properties are regulated by underlying molecular processes. In this report, we have used soft lithography to create morphologically polarized cells in order to examine rheological differences between the front and rear zone of an NIH 3T3 cell posed for migration. In addition, we trapped superparamagnetic beads with optical tweezers and precisely placed them at specific locations on the immobilized cells. The beads were then allowed to endocytose overnight before magnetic tweezers experiments were performed to measure the local rheological properties of the leading and trailing edges. Our results indicate that the leading edge has an approximately 1.9 times higher shear modulus than the trailing edge and that this increase in shear modulus correlates with a greater density of filamentous actin, as measured by phalloidin-staining observed through quantitative 3D microscopy.

* Department of Mechanical Engineering, MIT. Present address: Biochemistry and Molecular Biophysics Option, Caltech.
† Department of Biological Engineering, MIT
‡ Department of Chemistry and Chemical Biology, Harvard University. Present address: National Center for NanoScience and Technology, China.
§ Department of Chemistry and Chemical Biology, Harvard University
¶ Department of Biological Engineering and Department of Mechanical Engineering, MIT.
‖ Department of Biological Engineering and Department of Mechanical Engineering, MIT.

**Keyword:** cytoskeletal stiffness, microcontact printing, magnetic trap, optical tweezers; migration

## 1 Introduction

Cellular locomotion is a very complex process requiring the concerted coordination of many biochemical pathways. During migration on surfaces or in tissue matrices, the cell body becomes polarized in the direction of motion, resulting in a leading protruding edge and a trailing retracting edge. These changes in cell morphology have been related to changes in actin dynamics; particularly in the leading and trailing edges where actin is actively polymerized and depolymerized, respectively. Recent studies have shown that the mechanical properties of cells are correlated to actin networks (1); however, the rheology of polarized migrating cells has never been measured. In this report, we use soft lithography techniques in combination with optical tweezers and magnetic tweezers to control the shape of adherent cells and probe the location-dependent rheological properties of cells primed for migration.

Even though there is a rich literature on actin dynamics as well as on the molecular biology factors affecting cell polarization and migration (2, 3, 4, 5), there is very little known about the rheology of migrating cells. In fact, the fundamental question of whether cells become softer or stiffer during migration is subject to considerable debate (5, 6). In addition, the processes by which underlying molecular events give rise to changes in cellular mechanical properties and coordinated motion are not well understood (5, 7). Furthermore, it is now accepted that the interplay between mechanics and biochemistry, a process known as mechanotransduction in which the mechanical state of a

cell can heavily influence or trigger various signal transduction cascade pathways, is crucial for cellular survival. Therefore, an improved understanding of the rheology of migrating cells has implications for many biomedical problems, such as the cause of cardiovascular diseases and the development of tissue engineering constructs where cell migration is required to populate the artifical tissue (8, 9). Other areas to benefit from a better understanding of the rheology of cellular migration include a wide variety of fundamental processes ranging from wound healing to blood vessel formation (7).

A variety of methods, such as micropipette aspiration (10), cell poking (11), magnetic twisting cytometry (12), laser (13) and magnetic tweezers (14), atomic force microscopy (AFM) (1), and laser tracking microrheology (15), have been employed to probe the rheological properties of cells. In addition, optical tweezers have also been used to study membrane tethers (16). These techniques have made enormous contributions to the field of cellular rheology; however, the measurements obtained with these approaches have their own unique limitations and differences. For example, cell poking and micropipette aspiration only measure the bulk properties of cells and cannot measure local rheological differences within cells. Similarly, particle tracking methodologies (both passive and active approaches), are not suited for long experiments because the tracer particle location is random and may unexpectedly leave the region of interest. Because cellular rheological measurements often depend on the method employed, there is a need to develop better approaches to probe cellular mechanical properties. It is also desirable to have a more controlled assay using micropatterning to generate geometrically identical cells for more consistent rheological measurements (see companion paper, (17)).

In order to better measure the local intracellular rheological properties for a cell poised for migration, we use cells polarized using microfabrication and a magnetic microrheometer combined with optical tweezers. Magnetic rheometry is typically employed to study the rheology of cell because they are capable of accessing the high forces, on the order of nN, needed to deform cellular structures. However, they are not capably of stably trapping and placing objects at desired locations. Conversely, optical tweezers provide precise positioning ability, but they are best suited to probe the force regimes experienced by single molecules at the pN level and thus cannot provide the high forces needed to measure the full range of cellular rheological properties. In our approach, fibronectin coated superparamagnetic beads are first trapped and positioned with optical tweezers at the desired location of immobilized cells. The beads are then allowed to endocytose and later pulled upon with magnetic tweezers.

Optical tweezers offer high spatial resolution and, to the best of our knowledge, is the only reliable way to precisely place magnetic beads at specific locations on the cell. Optical trapping of magnetic beads is challenging due to their strong scattering and absorption properties (18, 19). This limitation can be overcome by trapping magnetic beads at low powers, a desired situation because it also limits damage to biological samples due to thermal and optical effects (20). Magnetic tweezers is a complementary method that can generate the sufficiently high forces needed for local rheological measurements without permanently damaging the cell of interest (21). Because the measured cellular strain field decays quickly from the location of the bead (22), the combined optical and magnetic tweezer approach provides a local as opposed to global measure of cellular rheology.

Even though it is widely accepted that the cellular cytoskeleton continuously remodels during migration, the exact mechanism for cell movement remains elusive. Nevertheless, of the main cytoskeletal components, actin has been heavily implicated in playing a decisive role in the generation of motion. It is known that actin polymerization occurs on the leading edge and depolymerization occurs on the trailing edge of a migrating cell. In addition, a variety of different models such as Brownian ratchet and motor-based motion have been proposed to explain how actin-based motion is generated (23, 24). However, these hypotheses have remained largely untested in living cells due to the absence of a noninvasive measurement

technique capable of measuring local rheological properties. (5, 25). Since much polymerization occurs at the leading edge, we hypothesize that it has a higher polymerized actin density (volume of actin/total cell volume) and therefore a higher Young's modulus. We focus our attention on the actin cytoskeleton because purified networks of actin polymers exhibit a higher shear modulus than networks containing microtubules or intermediate filaments and actin microfilaments are believed to be primarily responsible for the stiffness of the cell (26). In addition, AFM results by Haga, et al, 2000, have shown that elasticity maps of NIH3T3 fibroblast cells correlate mainly with the presence of the actin network. While microtubules and intermediate filaments may also be involved in regulating cytoskeletal rheology, we hypothesize that their influences are of secondary effect.

It is possible to study migrating cells in 2D culture but the motion of the cells can complicate bead placement and rheological measurements. Further, we have recently shown micropatterning reduces the variances in cellular mechanical property measurements by a factor of $\sim$4 as compared to unpatterned cells (companion paper, (17)). We employ micropatterning to further increase the reliability of our cell mechanics measurements. A recent study by Jiang, et al (2005), has demonstrated that imposing a morphologically polarized teardrop form on a cell using microcontact printing is sufficient to direct cell migration (27). We therefore generate a cell poised for migration by growing cells on teardrop shaped micropatterned islands. Because upon electrochemical desorption cells migrate off the patterns in the direction of the blunt end of the teardrop (27), beads placed on the blunt edge were defined as being on the edge in the direction of migration or the leading edge while beads on the sharp edge were defined as being on the trailing edge.

In this report, we first describe the combination and the performance of an optical trap and a magnetic microrheometer for cell mechanics measurements. We subsequently describe our study of micropatterned cells posed for migration using this system. To validate our hypothesis that regional variations in the rheological properties of migrating cells are due to a difference in local polymerized actin density, a quantification of regional polymerized actin density using confocal microscopy will be shown.

## 2 Materials and Methods

### *2.1 Substrate preparation*

Micropatterned substrates were created as previously described (28). Briefly, a 130 Å-thick layer of gold was deposited on the coverslip bottoms of Bioptechs culture dishes (Bioptechs, Butler, PA) using electron-beam vapor deposition. To promote the adhesion of the gold to glass, 30Å of titanium was first evaporated onto the dish. To create the polydimethylsiloxane (PDMS, Sylgard 184, Dow Corning, Midland, Michigan) stamp used for microcontact printing, negative photoresist (SU8-2015, Microchem, Newton, MA) was spin-coated for 35 seconds at 1500 rpm onto a 4" silicon wafer. The photoresist was then baked on a hotplate at 65$^o$C for 1 minute and 95$^o$C for 2 minutes. The photoresist was exposed to UV light for 12 seconds through a transparency photomask (Output City, Poway, CA) containing teardrop shapes to create the photoresist master. Following exposure, the wafer was post-baked again at 65$^o$C for 1 minute and 95$^o$C for 2 minutes. The unpolymerized photoresist was washed away with propylene glycol monomethyl ether acetate (PGMEA, Microchem, Newton, MA) and the wafers were silanized for 15 minutes to prevent the PDMS from sticking. PDMS was poured on the bas relief photoresist structure and baked in an oven for 2 hours at 65$^o$C. The PDMS stamp was then peeled off and coated with 2 mM hexadecanethiol (Sigma Aldrich, St. Louis, MO) in ethanol. Excess solvent was removed by evaporation in a stream of nitrogen, and the stamp was pressed onto the gold coverslip for 30 seconds. The stamp was then gently peeled off and the bottom of the dish covered with 2mM of a polyethyleneglycol (PEG)-terminated alkanethiol for 30 minutes. Afterwards the dishes were rinsed once with ethanol and once with phosphate buffered saline (PBS) solution (Invitrogen Life Technologies, Carlsbad,

CA).

### 2.2 Cell culturing and plating

Cells were cultured according to instructions provided by the American Type Culture Collection (ATCC). NIH 3T3 fibroblasts (ATCC, Manassas, VA) were grown using high glucose Dubecco's Modified Eagle Medium (DMEM) supplemented with 10% v/v bovine calf serum (Invitrogen Life Technologies, Carlsbad, CA) and 1% penicillin/streptomycin in 10 $cm^2$ tissue cultures plates in an incubator at 37°C until 70% confluent. Cells were split in a laminar flow hood where the media was vacuum aspirated off with a sterile pipette and 2.5 mL of trypsin-EDTA was added. The cells were placed back into the incubator for 5-7 minutes until they disassociated from the bottom of the plate. An equivalent amount of serum-containing media was added to inactivate the trypsin. The solution of media and cells was gently mixed using a 5-mL pipette for several minutes until a homogeneous suspension of cells was obtained. The desired quantity of cells was added to a new tissue culture plate for continued propagation and placed back into the incubator.

To plate the cells, 0.5 mL of 0.25 $\mu$g/mL of human plasma fibronectin (Sigma Aldrich, St. Louis, MO) in PBS was placed in each stamped dish for one hour at 37°C. The fibronectin was aspirated out, while the desired number of cells/mL was simultaneously loaded. Approximately 30,000 cells were added per dish.

### 2.3 Actin staining

For imaging, cells were fixed with 3.7% formaldehyde (Z-fix, Anatech LTD, Battlecreek, MI) and their F-actin stained with Alexa Fluor 488-conjugated phalloidin (Molecular Probes, Eugene, Oregon) according to protocol provided by Molecular Probes. The media was first aspirated and the cells were washed twice with PBS. Z-fix was added for 10 minutes and then removed by aspiration. The Bioptechs dishes were washed again twice with PBS and a solution of 0.1% Triton X-100 was added for a total of 5 minutes to allow for entry of the dye. Triton X-100 was removed and the bioptechs dishes were washed twice with PBS. The dishes were soaked then in a 1% bovine serum albumin (BSA) solution for 30 minutes to reduce non-specific binding. The staining solution consisting of 200 $\mu$L of PBS and 15 $\mu$L of methanolic dye solution was then added to each dish for 20 minutes after which the dishes were washed again twice with PBS, once with distilled water, and gently blown dried with nitrogen.

### 2.4 Magnetic bead preparation

Paramagnetic polystyrene beads (4.5 $\mu$m diameter, Dynal, Oslo, Norway) with a tosyl-activated coating were covalently conjugated to fibronectin. The solution containing the magnetic beads was placed on top of a magnet to draw the beads to the bottom. The storage solution was then removed by aspiration and the beads washed once in a borate buffer solution with a pH of 9.4. Fibronectin was added (15 $\mu g/10^7$ beads) and the solution was gently agitated for 10 minutes at 37°C. BSA was added until its concentration was 0.1%, and the entire mixture was agitated for 48 hours at 37°C. The beads were washed three times with 0.1% BSA in PBS, and once with Tris buffer with 0.1% BSA (pH 8.5). Prior to use, the beads were mixed in 1% BSA in PBS for 5 minutes, and resuspended in media.

### 2.5 Optical tweezer setup

The optical tweezers instrument (Figure 1) is based on a custom fitted DIC inverted microscope and employs a 975 nm light source (Corning Lasertron, Bedford, MA) as the trapping laser. Similar to previous designs (29, 30), trapping capabilities were achieved by guiding the trapping laser into the microscope objective (Nikon, 100X Plan Apo, 1.4NA) via a dichroic mirror positioned directly underneath the objective that reflects only near infrared light. In this design, double-trap capabilities were achieved by splitting and recombining the main laser line with two polarizing beam-slitting cubes (CVI). The amount of power delivered to each trap was controlled with a half-waveplate. High efficiency trapping was ensured by adjusting the laser diameter to a size comparable to that of the objective pupil. All bright field

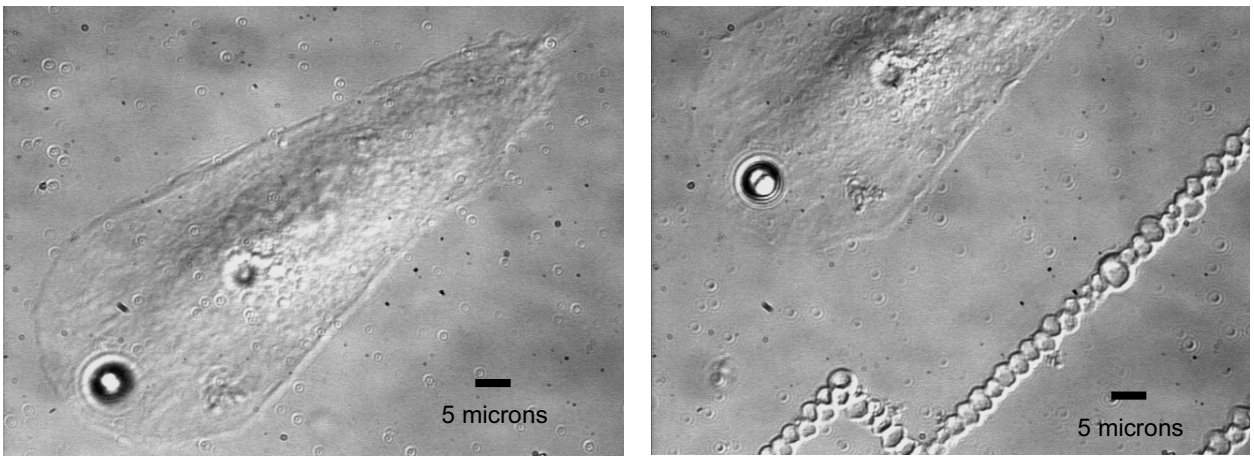


Figure 2: A magnetic bead is precisely positioned by optical tweezers on the leading edge of a teardrop patterned cell. The picture on the right shows how marking of the gold substrate by burning allows for ready identification of the cell in subsequent experiments.

imaging was done on a CCD camera.

Beads were initially placed on and bound to the cells (Figure 2) by holding the beads for approximately 15 minutes with a power of 1mW. Laser powers were measured before the beam entered the microscope. After binding the beads to the appropriate cell region, a box around the cell of interest was drawn for later identification (and bead manipulation with magnetic tweezers) by burning the gold surface with at least 55 mW of power. To calibrate the trap stiffness, the microscope stage was manually moved at a constant velocity, as confirmed by an independent laser-based stage position senor, and bead displacements from the center of the optical trap were monitored using a custom particle-tracking program (31). In addition to optical losses through the objective, the gold and titanium-coated plate was observed to only transmit approximately 15 % of the laser light. The optical trap was calibrated by using the Stokes drag method (32) and the stiffness of the trap was calculated to be approximately 0.28 fN/nm for 4.5 micron superparamagnetic beads at 4mW of power.

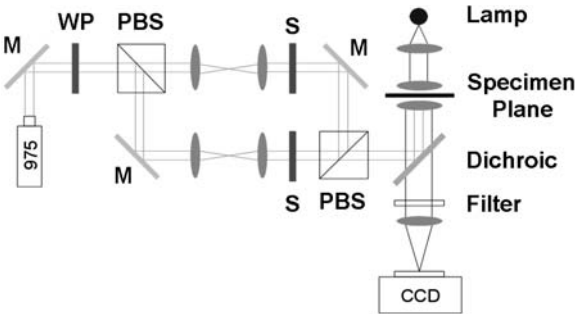


Figure 1: Optical tweezers schematic. M = mirror, PBS = polarizing beam splitter, S = shutter, WP = half-waveplate. Two optical traps were formed by splitting and recombining a 975 nm laser line and guided them into the objective with a dichroic mirror. One of the traps was formed with low power, $\sim$ 5 mW, and was used to trap superparamagnetic beads and position them on specified surface or cellular locations. After the beads were immobilized on cells, the other trap was formed with high laser power, > 55 mW, and was used to mark the substrate around the cell of interest for later identification and manipulation with magnetic tweezers.

### *2.6 Magnetic trap setup*

#### *2.6.1 General principles of a single pole magnetic trap*

A single pole magnetic trap was developed by Bausch, et al in 1998 (33) and has the advantage over other techniques of being able to exert nano-Newton level forces on 4.5 micron paramagnetic beads. These high forces permit cytoskeleton deformation in cells such as fibroblasts with elastic

moduli on the order of $10^3 - 10^4$Pa. The trap is an electromagnet that generates a magnetic field exerting a constant force $\vec{F}$ on a paramagnetic object:

$$\vec{F} = \frac{1}{2}\mu_0 \nabla \left(\vec{m} \cdot \vec{H}\right) \quad (1)$$

where$\mu_0$ is the permeability constant, $\vec{m}$ is the magnetization of the particle, and $\vec{H}$ is the external magnetic field strength. Generally paramagnetic as opposed to ferromagnetic beads are chosen as they are only magnetized when the magnetic field is turned on and so they do not aggregate (Bausch 1999). The beads are coated with fibronectin which allows them to be indirectly attached to the actin cortex via integrin receptors on the cell membrane. By varying the current through the electromagnet, the amount of force applied to the bead may be controlled.

The magnetic trap (Figure 3) was constructed following the design of Huang, et. al (34) which modified Bausch's design using finite element simulations to maximize the force level. A ferromagnetic CMI-C rod (Cold Metal Products Inc) was machined and heat treated to improve its magnetic properties (35). The trap was wrapped approximately 550 times with 21 gauge copper wire which was sealed in epoxy.

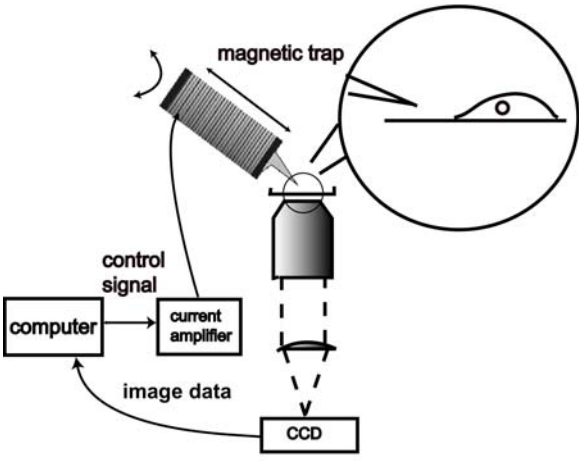


Figure 3: Magnetic trap schematic

A computer-controlled current applied through the coil generated a magnetic field that exerts force on the magnetic beads. The displacement of the bead over time in response to a step force was recorded to determine the effective stiffness of a cell. To calibrate the trap, a force was applied to a magnetic bead in a solution of known viscosity (12,500 cenststokes) (polydimethylsiloxane) (Sigma Aldrich, St. Louis, MO). The force increases exponentially as the distance from the bead to the tip decreases (36). Images were recorded at 30 fps using a CMOS camera (Silicon Imaging, Costa Mesa, CA). The steady state velocity of the bead was found by measuring the displacement over time using a custom particle-tracking program described previously (31) written in Matlab (Mathworks, Natick, MA).

For experiments in the cell, the tip of the magnetic trap was placed in the same focal plane as the bead. Cells were kept at 37 $^{o}$C through the use of both a temperature-controlled stage (Delta TC3, Bioptechs, Butler, PA), and an objective heater (Bioptechs, Butler, PA). For each experiment, a 5-second step-forcing function of approximately 20 nN of force was applied.

## 3 Results and Discussion

### *3.1 Demonstration of Spatial Positioning using the Optical-Magnetic Rheometer*

Since their initial demonstration, optical tweezers have been widely adopted to noninvasively explore the effects of mechanical forces on biological systems at the molecular and cellular length scales. In particular, optical tweezers have been used to study the mechanics of DNA and cellular membranes, the processivity of molecular motors, protein unfolding, and the strength of receptor-ligand interactions (37-42). Other applications include the manipulation of individual viruses, bacteria, organelles, and even complete cells. (43)

Stable trapping is commonly achieved by using a high numerical aperture objective to tightly focus an infrared laser beam. The interaction of the focused beam with freely diffusing particles gives rise to two forces: a scattering force and a gradient or restoring force. The scattering force is destabilizing and pushes objects along the direction of the incident light, while the gradient force, resulting from refraction, pulls particles toward the high

intensity focus of the laser beam. The stability of the trapping phenomenon hinges on the dominance of the restoring force over the scattering force (44)

Optical tweezers can trap small dielectric microspheres approximately 1 micron in diameter with exquisite force and position resolution, typically on the order of picoNewtons and nanometers, respectively. Although commonly used to exert forces on the order of 10 pN, they have been shown capable of applying loads of up to 100 pN in particular arrangements (45, 46). These force levels are suitable for many applications, but, unfortunately, they have proven insufficient to appropriately study the full range of cellular rheological properties. We therefore combine the trapping capabilities of optical tweezers with the high-force capabilities of magnetic tweezers probe the rheological properties of some cells.

Several reports have demonstrated optical tweezers capable of trapping metallic beads. A particular study found that Rayleigh size gold particles (36 nm) are trapped stronger than similarly sized latex particles (32). The dominance of the gradient force for these particles was attributed to the larger polarizability of metals; however, unfavorable force balances are expected for particles larger than 40 nm (32). This result is at odds with a later report stating that superparamagnetic and polystyrene beads with 2.6 $\mu$m diameters can be optically trapped with the same force (18, 19). This study featured a magneto-optic trap in which a custom magnetic manipulator was built around a water-immersion objective to rotate optically-trapped superparamagnetic particles. Similar magneto-optical tweezers arrangements have also been developed, with a particular design used to intertwist two DNA molecules attached to a paramagnetic bead (47) and another to measure liquid-crystal-mediated forces between spherical superparamagnetic beads (48). Here we develop technology to combine the trapping capabilities of optical traps with the high-force exerting capabilities of magnetic tweezers. In Figure 4 we demonstrate the trapping and positioning capability of our optical tweezers for 4.5 micron diameter superparamagnetic beads in a predetermined pattern (MIT). We then use both of these instruments to precisely trap and position superparamagnetic beads on different locations of adherent cells. After endocytosis, we use magnetic tweezers to probe the location-dependent rheological microenvironment of the cells.

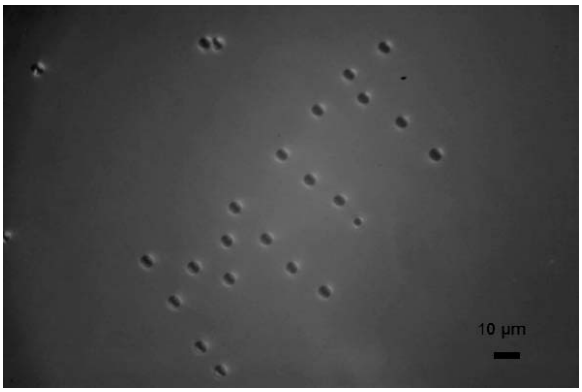


Figure 4: 4.5 micron diameter superparamagnetic beads precisely positioned to read MIT on a gold surface using optical tweezers.

### *3.2 Quantification of intracellular rheological variations*

Fibronectin coated magnetic beads were optically trapped and brought into contact with the cell at the desired location until the bead adhered to the membrane. The cells were then put back in the incubator overnight to let the beads endocytose. Regions of the cell (Figure 6a) rather than specific locations were defined as once the beads were endocytosed the cell tended to internally transport the bead slightly away from where it initially bound. Nonetheless, the beads tend to remain close to where they are placed within the time scale of our experiment.

The internalization of the beads was confirmed after 12 hours using confocal microscopy (Figure 5). This is an important result because bead internalization eliminated the effect of bead rolling which occurs when beads are exclusively attached to the cell membrane (22). This situation has been shown to contribute to a large source of error for this class of magnetic based rheometers (22).

Once beads were internalized they were pulled

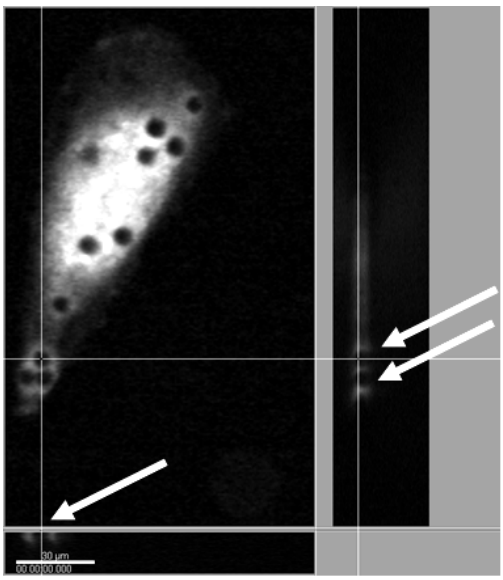

Figure 5: Demonstration that beads are internalized on teardrop micropatterns. Cells were stained with the celltracker green. Beads were allowed to internalize for 12 hours after which confocal images were taken and 3D reconstruction was performed. The view on the right represents a side view (vertical cut) and the view on the bottom represents another side view (horizontal cut). The crosshair is positioned on one bead. This bead is seen in the orthogonal views as linked by the cross hair.

upon with 20 nN $\pm$ 1 nN of force for five seconds. To avoid contamination and cell morbidity, cells were only outside the incubator for a maximum of thirty minutes. In the actual experiments, contrary to the picture shown in Figure 5, only one bead per cell was placed to avoid the effects of bead-bead interactions. Each cell resulted in one data point. The bead displacement as a function of time was recorded and an analytical expression was obtained by curve fitting to a Voigt model in series with a dashpot. The regional shear modulus was calculated as previously described (See companion paper, (17) and (49)) by assuming a bead embedded in a linear, infinite, isotropic, viscoelastic medium where $x(\omega)$ is the bead displacement in the frequency domain is $f(\omega)$ is the applied force in the frequency do-

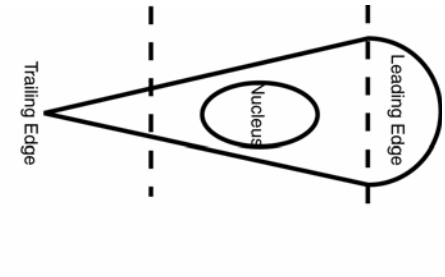


(a)

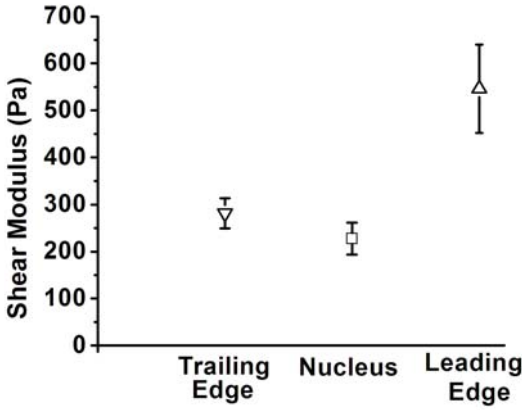


(b)

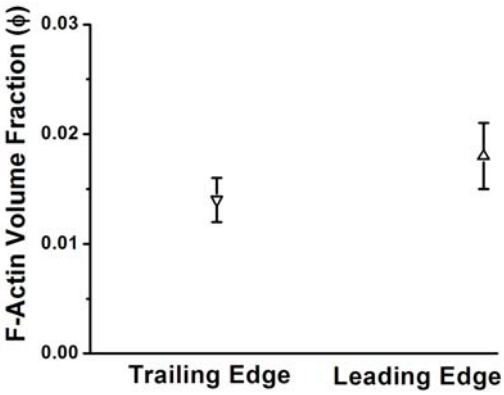


(c)

Figure 6: (a) Schematic of cell with different regions defined. The teardrop is 103 microns long and 30 microns in diameter at the widest part (b) Shear modulus at different locations of the cell. n = 5 for each case per cell. Error bars represent the standard error of the mean. (c) F-actin volume fraction (fraction of space occupied by actin) at different locations of the cell.

main.

$$G^*(\omega) = \frac{f(\omega)}{6\pi R x(\omega)} \quad (2)$$

Despite the close presence of the cell boundary (Figure 5), these assumptions that a bead is embedded in a linear, infinite, isotropic, viscoelastic medium are widely assumed in all bead based rheological calculations as there exists at present no analytic expression which takes into account the boundary conditions for the calculation of the shear modulus. A versatile, precise, and efficient finite element method to account for such complicated boundary conditions has yet to be developed. As current rheological methods are unable to separate out the contributions of the membrane from the cytoskeleton, we view the shear modulus taken from this calculation as a lumped modulus which takes into account all contributions. Briefly, as shown in equation (2) the Fourier transform of the step force was taken and divided by the Fourier transform of the analytic expression for the bead displacement to calculate the frequency dependent complex shear modulus $G*(\omega)$. The real part of (2) was taken and evaluated at 0.05 Hz to obtain a single value for the shear modulus. The value 0.05 Hz was chosen to be much longer than the relaxation time of the cell which was found to be $\sim$ 1 s (See (17)).

The resulting shear modulus at the leading edge was found to be a factor of $\sim$1.9 stiffer than the trailing edge and a factor of $\sim$2.4 stiffer than the nucleus (Figure 6b). Earlier experiments performed on cells adhered to micropatterned islands of increasing size found that their shear modulus was biphasic with pattern diameter while cell height was monotonic (See companion paper, (17)). From this we conclude that cell height while potentially a contributor is not the determining factor of cellular shear modulus. The result that the nucleus is softer than the leading edge qualitatively confirms AFM results by Haga and coworkers with the exception being that AFM results report that the nucleus is a factor of 10 softer than surrounding regions. We attribute this difference in part to the fact that the AFM probes the surface whereas the optical-magnetic trap probes the interior of the cell surrounding an endocytosed bead.

Our results is consistent with previous AFM surface measurements, (1, 25) that adherent cells are mechanically differentiated in their different regions. Work by Kole et al, 2004, has demonstrated using intracellular microrheology that the leading edge of Swiss 3T3 fibroblasts is stiffer than the perinuclear region. We observe in addition to the differences in stiffness between the leading and trailing edge, that the nuclei of NIH3T3 fibroblast cells are softer than the surrounding cytoplasm by a factor of $\sim$2.4. Our values for the Young's modulus at the leading edge are on the order of 1000 Pa which agrees with the modulus needed by the Brownian ratchet model to predict the forces generated from the polymerization of actin filaments in the lamellipodia (5). In addition our work demonstrates that a cell posed for migration is softer than a quiescently resting cell (stiffness values determined in companion paper, (17)) demonstrating the mechanical properties change upon the onset of migration. These results contradict with results by Kole et al, 2004, who obtained Young's moduli on the order of 10 Pa in contraction with the Brownian ratchet model and whose stiffness results for quiescent cells were larger than for migrating cells.

### *3.3 Quantification of F-actin structural parameters*

We hypothesize that the change in shear modulus occurs as a result of changes in the volume fraction of polymerized actin. To quantify the amount of F-actin in the cell, teardrop patterned cells were fixed and their F-actin stained with AlexaFluor488-Phalloidin. Two dimensional slices were taken using a spinning disk confocal microscope (Perkin Elmer Ultraview, Wellesley, MA), spanning every 100 nm and the resulting three-dimensional image stack deconvolved using Huygens Essential software to remove the out- of-focus light. A 100x Plan Apo Nikon objective with a numerical aperture of 1.45 was used for imaging. The images were background subtracted and a consistent threshold applied to determine the presence of actin. To calibrate fluorescent intensity with a value for the

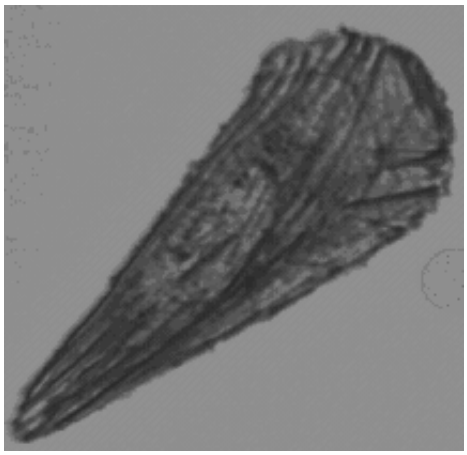

Figure 7: 3D reconstruction of the actin distribution inside a teardrop patterned cell. The black represents stress fibers which appear more densely around the edges of the cell. Image was created using Imaris software (Bitplane AG, St. Paul, MN).

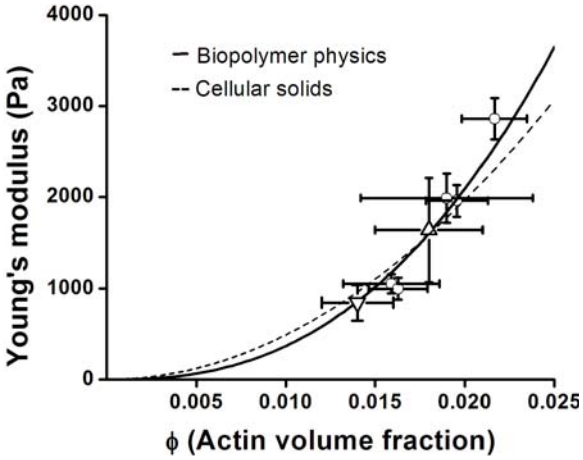


Figure 8: Young's modulus as a function of actin volume fraction. The triangles denote the data from the leading (right side up triangle) and trailing (upside down triangle) edge of the teardrop shaped cells. The circular (◯) points refer to data taken from patterned circular cells 10, 20, 30, 40, and 50 microns in diameter (See companion paper, (17)). The line fits to an exponent dependence of 5/2. For the teardrop patterned cells, there were 5 stiffness data points taken at each location. For the circular patterned cells there were 20 stiffness measurements taken at each location. For the actin density measurement, $n = 20$ for all cases. Error bars represent the standard error of the mean.

amount of actin present in each region of the cell, a solution containing a known concentration of actin which was labeled in the same manner as the cells was used (See companion paper, (17)).

To get a measure of the volume fraction of actin within each region, the volume of the largest rectangle that could be inscribed in each region was used. The resulting F-actin volume fraction data along with the corresponding Young's modulus from the magnetic trap data (Figure 8) was superimposed on a non-linear curve fit (Mathematica, Experimental Data Analyst) of the data previously obtained from cells on five different sized circular islands (companion paper, (17)) on an exponent of 5/2 and 2. The choice of exponents for the non-linear curve fit was based on the biophysical polymer model developed by Mackintosh and coworkers (50) which predicts a 5/2 dependence of the Young's modulus on actin volume fraction and the cellular solids model developed by Satcher and Dewey (51) which predicts a quadratic dependence of Young's modulus on actin volume fraction. To convert between shear modulus (G) and Young's modulus modulus (E) it was assumed that the cell was incompressible (E=3G).

From Figure 8, the teardrop data appears to fit with previous the circular patterned data very well. This data together appears to validate our hypothesis that polymerized actin density the primary determinant of cell local rheology. The polymerized actin density alone, to the first order, is sufficient to predict the Young's modulus and that the filament orientation seems to play little role in determining the cell stiffness. The investigation of filament orientation by Hu, et al, 2004 (52), seems to indicate that the fiber orientation effect is also secondary. Recently Théry et al, (53, 54), has investigated the role of adhesion area anisotropy on fiber orientation, but not on the resulting rheological dependence. It would be interesting to investigate the effect of filament orientation but substantial improvement on our instrumentation accuracy is needed to delineate the

effect of filament orientation on cell rheology.

A potential concern of this work relates to the fact that the leading edge of the cell is substantially thicker ($\sim$ factor of 2 greater) than the trailing edge. One may argue that the differences in cell rheology measured are due to a different in cell height or the proximity of the membrane to the tracer bead. We would like to assert that cell height and membrane proximity both play only a secondary role in cell rheology as compared to polymerized actin density. First, as demonstrated in our companion paper, cell rheology shows biphasic behavior while cell height is monotonic. Second, in the companion paper, we show that the shear modulus of the cell increases with decreasing cell height (large cell diameter). In this study, we show that the leading edge of the cell with large cell height shows a higher shear modulus than the trailing edge which is thinner. Finally, the excellent correlation of both cell area data (companion paper) and region rheology data of a migrating cell (this paper) with polymerize actin density reinforces the validity of our hypothesis.

## 4 Conclusions

We have examined the rheological variations between the leading and trailing edges of a cell posed for migration by combining the spatial precision of optical tweezers with the high force capabilities of magnetic tweezers. Although it is known that the cytoskeleton reorganizes for coordinated cellular movement to occur, little is known about how this reorganization translates into a mechanical property. It remains unknown whether a cell softens or stiffens during migration and a variety of hypotheses exist on how rheological changes result in whole cell movement. Our study supports the fact that a migrating cell is mechanical differentiated and has demonstrated that the leading edge of a polarized cell is significantly stiffer than the trailing edge. We have further shown that the nucleus is softer than the surrounding cytoplasm and that a cell poised for migration while not actually moving can be softer than a quiescently resting cell (see companion paper). In addition, the values we obtain for the Young's modulus at the leading edge are on the order of 1000 Pascals which is the stiffness the Brownian ratchet model requires to predict the force generated by actin polymerization. This particular finding of ours contradicts with the work of Kole, et al, 2004 that found the stiffness at the lamellipodia to be on the order of 10 Pascals and which found that a quiescent cell to be softer than a migrating cell. The variation in stiffness between the leading and trailing edges correlates with local actin volume fraction measurements with the dependence of Young's modulus and actin volume fraction appearing to agree with either a 5/2 power law as predicted by the biopolymer physics model or a quadratic dependence as predicted by the cellular solids model. Micro-mechanical models of the cell such as the biopolymer physics and cellular solids model provide a molecular level explanation for more global properties such as stiffness.

Our study has also demonstrated that we can apply a combination of optical-magnetic tweezers to investigate subcellular rheology. We would like to note that when the beads are internalized the cell internally transports the bead an additional amount so at this point the bead location is not precisely pre-determined, yet this motion appears to be small. As such, for endocytosed beads, we define regions of the cell (Figure 6a) rather than specific locations. With this technique, however, we are directly studying the cells we select rather than mixing cells and beads and choosing the ones available. This reduces randomness and interference due to other beads being present. Nevertheless, since the height of the cell and the bead size is comparable to the cell thickness, it should be noted that the underlying theory underlying shear modulus calculation is not rigorously valid. This is an inherent limitation with all bead based microrheological techniques and as such our data is a regional Young's modulus which includes contributions from the membrane as well as the cytoskeleton. The use of finite element to more precisely determine cellular shear modulus for endocytosed beads is a subject for future investigation (22).

**Acknowledgements:** We would like to thank Jorge Ferrer for assistance with the actin filament gels. This work was supported by NIH P01HL64858 and a NSF graduate research fellowship (Judith Su). Ricardo Brau acknowledges the National Institute of General Medical Sciences Biotechnology Training Program and the Lemelson Foundation for financial support. The salary of Xingyu Jiang was provided by NIH GM065364.

## References

1. **Haga, H.; Sasaki, S.; Kawabata, K.; Ito, E.; Sambongi, T.** (2000): *Ultramicroscopy*, 82(1-4), 253-8.
2. **Lauffenburger, D. A.; Horowitz, A. F.** (1996): *Cell*, 84, 359-369.
3. **Mitchison, T. J.; Cramer, L. P.** (1996): *Cell*, 84, 371-379
4. **Pollard, T. D.; Borisy, G. G.** (2003): *Cell*, 112, 453-465.
5. **Kole, T. P.; Tseng, Y.; Jiang, I.; Katz, J. L.; Wirtz, D.** (2005): *Molecular Biology of the Cell*, 16, 328-338.
6. **Cramer, L. P.; Briggs, L. J.; Dawe, H. R.** (2002): *Cell Motil. Cytoskeleton*, 51, 27-38.
7. **Munevar, S.; Wang, Y. L.; Dembo, M.** (2003): *Journal of Cell Science*, 117, 85-92.
8. **Chicurel, M.** (2002): Cell Migration Research is on the Move. *Science*, 295(5555), 606-609.
9. **Ridley, A. J.; Schwartz, M. A.; Burridge, K.; Firtel, R. A.; Ginsberg, M. H.; Borisy, G.; Parsons, J. T.; Horwitz, A. R.** (2003): *Science*, 302, 1704-1709.
10. **Evans, E.; Yeung, A.** (1989): *Biophysical Journal*, 56, 151-160.
11. **Zahalak, G. I.; McConnaughey, W. B.; Elson, E. L.** (1990): *J. Biomech Eng.*, 112(3), 283-94.
12. **Fabry, B.; Maksym, G. N.; Butler, J. P.; Glogauer, M.; Navajas, D.; Fredberg, J. J.** (2001): *Phys Rev Lett.*, 87(14), 148102.
13. **Choquet, D.; Felsenfeld, D. P.; Sheetz, M. P.** (1997): *Cell*, 88, 39-48.
14. **Bausch, A. R.; Möller, W.; Sackmann, E.** (1999): *Biophysical Journal*, 76, 573-579.
15. **Yamada, S.; Wirtz, D.; Kuo, S. C.** (2000): *Biophysical Journal*, 78(4), 1736-1747.
16. **Dai, J.; Sheetz, M. P.** (1999): *Biophysical Journal*, 77(6), 3363-3370.
17. **Su, J.; Jiang, X.; Welsch, R.; Whitesides, G. M.; So, P. T. C.** (2007): Geometric Confinement Influences Cellular Mechanical Properties I – Adhesion Area Dependence. *MCB: Molecular Cellular Biomechanics*, 4(2), 87-104.
18. **Sacconi, L.; Romano, G.; Ballerini, R.; Capitanio, De Pas, M.; Giuntini, M.; Dunlap, D.; Finzi, L.; Pavone, F. S.** (2001): *Optics Letters*, 26, 1359-1361.
19. **Romano, G.; Sacconi, L.; Capitanio, M.; Pavone, F. S.** (2003): *Optics Communications*, 215, 323-331.
20. **Neuman, K. C.; Chadd, E. H.; Liou, G. F.; Bergman, K.; Block, S. M.** (1999): *Biophysical Journal*, 77(5), 2856-2863.
21. **Mills, J. P; Qie, L.; Dao, M.; Lim, C. T.; Suresh, S.** (2004): *Mech Chem Biosyst.*, 1(3), 169-180.
22. **Karcher, H.; Lammerding, J.; Huang, H.; Lee, R. T.; Kamm, R. D.; Kaazempur-Mofrad, M.** (2003): *Biophysical Journal*, 85(5), 3336-3349.
23. **Peskin, C. S.; Odell, G. M.; Oster, G. F.** (1993): *Biophysical Journal*, 65, 315-324.
24. **Mogilner, A.; Oster, G.** (1996): *Biophysical Journal*, 71, 3030-3045.
25. **Heidemann, S. R.; Wirtz, D.** (2004): *Trends Cell Biol.* 14, 160-166.

26. **Hvidt, S.; Heller, K.** (1990): *Physical Networks. Polymers and Gels*. (W. Burchard and S. Ross-Murphy, Ed.) London: Elsevier.

27. **Jiang, X.; Bruzewicz, D.; Wong, A. P.; Piel, M.; Whitesides, G. M.** (2005): *Proc. Natl. Acad. Sci. USA*, 102(4), 975-978.

28. **Whitesides, G. M.; Ostuni, E.; Takayama, S.; Jiang, X.; Ingber, D. E.** (2001): *Annu. Rev. Biomed. Eng.*, 3, 335-73.

29. **Lang, M. J.; Fordyce, P. M.; Engh, A. M.; Neuman, K. C.; Block, S. M.** (2004): *Nature Methods*, 1(2), 133-139.

30. **Brau, R. R.; Tarsa, P. B.; Ferrer, J. M.; Lee, P.; Lang, M. J.** (2006): *Biophysical Journal*, 91(3), 1069-1077.

31. **Lammerding, J.; Kazarov, A. R.; Huang, H.; Lee, R. T.; Hemler, M. E.** (2003): *Proc. Natl. Acad. Sci. USA*, 100(13), 7616-7621.

32. **Svoboda, K.; Block, S. M.** (1994): *Optics Letters*, 19, 930-932.

33. **Bausch, A. R.; Ziemann, F.; Boulbitch, A. A.; Jacobson, K.; Sackmann, E.** (1998): *Biophysical Journal*, 75(4), 2038-2049.

34. **Huang, H.; Dong, C. Y.; Kwon, H-S.; Sutin, J. D.; Kamm, R. D.; So, P. T. C.** (2002): *Biophysical Journal*, 82(4), 2211-2223.

35. **Huang, H.; Kamm, R. D.; Lee, R. T.** (2004): *Am J Physiol Cell Physiol*, 287, C1-C11.

36. **Su, T-T. J.** (2004): MS thesis, MIT.

37. **Wang, M. D.; Yin, Y.; Landick, R.; Gelles, J.; Block, S. M.** (1997): *Biophysical Journal*, 72, 1335-1346.

38. **Raucher, D.; Sheetz, M. P.** (2000): *Journal of Cell Biology*, 148, 127-136.

39. **Asbury, C. L.; Fehr, A. N.; Block. S. M.** (2003): *Science*, 302, 2130-2134.

40. **Abbondanzieri, E. A.; Greenleaf, W. J.; Shaevitz, J. W.; Landick, R.; Block, S. M.** (2005): *Nature*, 438, 460-465.

41. **Litvinov, R. I.; Bennett, J. S.; Weisel, J. W.; Shuman, H.** (2005): *Biophysical Journal*, 89, 2824-2834.

42. **Cecconi, C.; Shank, E. A.; Bustamante, C.; Marqusee, S.** (2005): *Science*, 309: 2057-2060.

43. **Ashkin, A.; Dziedzic, J. M.** (1987): *Science*, 235, 1517-1520.

44. **Ashkin, A.** (1992): *Biophysical Journal*, 61, 569-582.

45. **Maier, B.; Potter, L.; So, M.; Seifert, H. S.; Sheetz, M. P.** (2002): *Proc. Natl. Acad. Sci. USA*, 99, 16012-16017.

46. **Dao, M.; Lim, C. T.; Suresh, S.** (2003): *Journal of the Mechanics and Physics of Solids*, 51, 2259-2280.

47. **Claudet, C.; Bednar, J.** (2005): *Applied Optics*, 44, 3454-3457.

48. **Kotar, J.; Vilfan, M.; Osterman, N.; Babic, D.; Copic, M.; Poberaj, I.** (2006): *Physical Review Letters*, 96, -.

49. **Schnurr, R.; Gittes, F.; MacKintosh, F. C.; Schmidt, C. F.** (1997): *Macromolecules*, 30, 7781-7792.

50. **Mackintosh F. C.; Kas, J.; Janmey, P. A.** (1995): *Physics Review Letters*, 75(4), 4425-4428.

51. **Satcher, R.; Dewey, C. F.** (1996): *Biophysical Journal*, 71, 109-118.

52. **Hu, S.; Eberhard, L.; Chen, J.; Love, J. C.; Butler, J. P.; Fredberg, J. J.; Whitesides, G. M.; Wang, N.** (2004): *Am J. Physiol Cell Physiol.*, 287, C1184-C1191.

53. **Théry, M.; Racine, V; Piel, M.; Pépin A.; Dimitrov, A.; Chen, Y.; Sibarita, J-B.** (2006): *Proc. Natl. Acad. Sci. USA*, 103, 19771-19776.

54. **Théry, M.; Jiménez-Dalmaroni, A.; Racine, V.; Borens, M.; Jülicher, F.** (2007) *Nature*, 447, 493-496.